Journal of Catalysis **182,** 313–327 (1999)
Article ID jcat.1998.2376, available online at http://www.idealibrary.com on IDEAL®

On the Promotion of Ag–ZSM-5 by Cerium for the SCR of NO by Methane

Zhijiang Li and Maria Flytzani-Stephanopoulos

Department of Chemical Engineering, Tufts University, Medford, Massachusetts 02155

Received June 17, 1998; revised December 4, 1998; accepted December 7, 1998

The promotion of Ag–ZSM-5 by cerium for the selective catalytic reduction (SCR) of NO with methane in the presence of an excess of oxygen was studied in this work. Ce–Ag–ZSM-5 catalyzes the CH_4-SCR of NO_x over the temperature range of 450–600°C. Rate measurements of NO reduction to N_2 under SCR conditions and of the competing CH_4 oxidation by O_2 (CH_4 combustion) show that incorporation of a small amount (1–1.5 wt%) of cerium into Ag–ZSM-5 enhances the activity and selectivity of the latter for the SCR reaction. Catalysts with low Ag exchange levels (<50%) were found to be more selective than those with high Ag loading, the latter being more active for CH_4 combustion. To examine the role of silver and cerium in the Ce–Ag–ZSM-5 system, the kinetics of the SCR reaction were complemented by studies of NO oxidation to NO_2, SCR of NO_2 by CH_4, and CH_4 combustion as well as catalyst characterization by STEM/EDS, HRTEM/EDS, XPS, and UV-VIS DRS techniques. Silver existed mainly as dispersed Ag^+ ions in low Ag-content (Ag/Al < 0.5–0.6) Ce–Ag–ZSM-5 samples, while nanoparticles of silver of ~10 nm size were also found on the surface of high Ag-content samples. The dispersed Ag^+ state was more active for the SCR reaction, while silver particles more effectively catalyzed the methane combustion reaction. Cerium was present in both the 3+ and 4+ oxidation states. The major functions of cerium suggested by the data presented in this paper are to catalyze the oxidation of NO to NO_2, suppress the CH_4 combustion, and stabilize silver in dispersed Ag^+ state. © 1999 Academic Press

Key Words: **reduction of nitrogen oxides; methane oxidation; methane; ZSM-5; silver; cerium.**

INTRODUCTION

Stricter NO_x emission standards recently adopted by many countries are driving the search for more effective and economical methods to control NO_x emissions from stationary and mobile sources. New opportunities for improvement have emerged following the discovery of new catalysts for the direct decomposition of NO_x and the selective catalytic reduction (SCR) of NO_x with hydrocarbons. The latter has sparked considerable scientific and industrial interest ever since it was first reported by Iwamoto *et al.* (1) and Held *et al.* (2). The most attractive feature of this NO_x reduction process, which distinguishes it from the previous NO_x reduction technologies using CO and H_2, is that the presence of oxygen in the exhaust stream is generally necessary for high conversion of NO_x to N_2, and excess oxygen may or may not be limiting depending mainly on the type of catalyst used.

Among various hydrocarbons, CH_4 is especially attractive as the NO_x reductant for application to power generation using natural gas as the feedstock (gas turbines) and to CNG engines/vehicles. Methane is typically more difficult to activate than other hydrocarbons. Catalysts active for the SCR of NO by higher hydrocarbons or oxygenates may not work or have much lower activity when methane is used as the reducing agent (3, 4). Although several single metal ion-exchanged zeolites, such as Co– (5, 6), Mn– (5), Ga– (6–8), In– (8, 9), and Pd–ZSM-5 (10), have been shown active for the SCR of NO by CH_4, the NO reduction rates over these catalysts are approximately one order of magnitude lower than the rate of the currently employed SCR of NO by NH_3 over vanadia–titania catalysts (11). Lack of durable catalysts with high activity at high gas space velocities and in the presence of water vapor and SO_2 has hurdled the application of this technology. Nevertheless, the search for new catalysts has continued unabated.

In both the SCR of NO_x by hydrocarbons as well as the direct NO decomposition, the steady-state activity and stability of certain single metal ion-exchanged zeolite catalysts may be improved by incorporation of a second metal ion in the zeolite. Alternatively, by proper selection of the two metals, new catalysts might be discovered for these catalytic processes. In an early study by Teraoka *et al.* (12) on bimetal exchanged catalysts for the SCR of NO by ethene, the coexistence of Ca, Co, or Fe with Cu ions in ZSM-5 was found to enhance the activity of Cu–ZSM-5 and to also expand the active temperature window. A similar promotion effect was also reported for the SCR of NO by propene over alkaline earth-promoted cerium ion exchanged ZSM-5 catalysts by Yokoyama *et al.* (13). Strontium was found to promote the catalytic activity and selectivity of the Ce–ZSM-5 catalyst significantly, although Sr–ZSM-5 itself was not active for the reaction. Modification of the coordination of Ce ions in the zeolite by the presence of Sr ions was discussed as the probable cause for the enhanced performance of the bi-metal catalyst. The effect of cocation on the catalyst performance for the same reaction under wet gas conditions was studied by Torre-Abreu *et al.* (14) over alkaline earth-promoted copper ion-exchanged mordenite.

0021-9517/99 $30.00

Improvement of catalyst stability under wet conditions by addition of Ba was observed. The authors further suggested that the catalyst deactivation could be prevented by choosing an appropriate cocation. In previous work carried out by our group, the promotion effect of alkaline earths and rare earths on Cu–ZSM-5 catalysts for the direct NO decomposition was shown under both dry and wet gas conditions (15, 16). Higher turnover frequencies of NO per copper site were measured over cerium or magnesium-promoted Cu–ZSM-5 catalysts. The wet gas activity of the bi-metal Ce–Cu–ZSM-5 catalysts for the direct NO decomposition was superior to that of unpromoted Cu–ZSM-5. A major function of cerium in Ce–Cu–ZSM-5 is to stabilize copper in dispersed form and suppress copper migration and aggregation in the zeolite channels. Stabilization of copper was also demonstrated by using La and Sr in Cu–ZSM-5 (17).

Recently, we examined the promotion effect of cerium on metal ion-exchanged ZSM-5 catalysts for the SCR of NO using methane as the reducing agent in the presence of excess oxygen (18, 19). Catalysts studied included some of those previously reported as active for the SCR of NO with CH_4, such as Co–, Mn–, Ga–, and In–ZSM-5, and others reported to activate CH_4 at relatively low temperatures, such as Ag– (20) and Pd–ZSM-5 (21). A significant synergistic effect was found over cerium-promoted silver ion-exchanged ZSM-5 (19). While neither Ce–ZSM-5 nor Ag–ZSM-5 showed high activity for the SCR reaction with CH_4, Ce–Ag–ZSM-5 displayed high activity over the temperature range of 450–600°C. A small amount of cerium (1.0–1.5 wt%) in ZSM-5 gave the maximum promotion and the conversion of NO to N_2 increased linearly with the silver exchange level up to ~60%. Previous reports of SCR activity of silver catalysts were limited to other organic reductants. For example, although silver supported on alumina and mordenite catalysts were found active and durable for the SCR of NO by propene in the presence of both water vapor and sulfur dioxide (22–24), they have not been reported as active for the SCR of NO with methane.

The aim of the present work was to further examine the promotion of Ag–ZSM-5 by cerium. Reaction rates were measured for the SCR of NO and NO_2 and for CH_4 combustion over a series of promoted and unpromoted Ag–ZSM-5 samples with various cerium and silver loadings. Characterization of selected fresh and aged catalyst samples by STEM/EDS, HRTEM/EDS, XPS, and UV-VIS diffuse reflectance spectrometry(DRS) was performed to correlate catalyst activity with structure and identify potential structural effects of cerium.

EXPERIMENTAL

Sample Preparation

Detailed procedures for the preparation of ion-exchanged Ag–ZSM-5, Ce–ZSM-5, and Ce–Ag–ZSM-5 catalysts were described in a previous paper (19). A Na–ZSM-5 with Si/Al = 13 (obtained from the Davison Chemical Division, W.R. Grace & Co.) was used as the parent zeolite. Ag^+ ion exchange was carried out at room temperature in the dark for 24 h using 200 ml of aqueous silver(I) nitrate solution (0.001 to 0.01 *M*) to exchange 2 g zeolite each time. After exchange, the sample was filtered, washed with deionized water, and dried at 110°C overnight in air. Heat treatment was performed at 500°C in air for 2 h. If necessary, the exchange was repeated two to three times before washing to reach high Ag^+ loadings. To prepare Ce–ZSM-5 samples, 0.0003–0.01 *M* cerium(III) nitrate solutions were used and the exchange was carried out at 80°C for 2 h. Ce–Ag–ZSM-5 samples were prepared by first exchanging the Na–ZSM-5 with cerium(III) nitrate and then silver(I) nitrate. Rinsing, drying, and calcination of Ce^{3+} exchanged samples were performed before Ag^+ exchange to stabilize a fraction of the cerium ions inside the zeolite (16). The final samples were analyzed by inductively coupled plasma emission spectrometry (ICP, Perkin–Elmer Plasma 40) to determine their elemental composition. Table 1 lists the samples prepared in this work, their corresponding ICP analysis, and their charge balance. In Table 1 the number in parentheses next to each element indicates the percent exchange level, assuming each Ag^+ ion exchanges one Na^+ ion and each Ce^{3+} ion exchanges three Na^+ ions. The latter may hardly be possible in high Si–Al zeolites. Rather, it represents the upper bound for Ce^{3+} ion exchange. The charge balance for each sample was computed as (3Ce + Ag + Na)/Al. This calculation may show an artificially high charge balance, i.e., (3Ce + Ag + Na)/Al greater than 1. On the other hand, protonation of some sites may be inferred by a charge balance less than unity (see Table 1).

Reaction Rate Measurements

Reaction rates were measured in a fixed bed microreactor system, consisting of a 1/4 inch O.D. quartz reactor tube, a temperature controller (OMEGA, CN2040), four mass flow controllers (Brooks, 5850E), and a HP 5890 gas chromatograph (GC) equipped with a thermal conductivity detector (TCD). A 10 ft, 1/8 inch O.D. 5A molecular sieve column operated at 40°C was used to separate O_2, N_2, CH_4, NO, and CO. Source gases were certified gas mixtures (Airco): 2.94 or 0.476% NO in He, 0.716% NO_2 in He, 4.87% CH_4 in He, and 10.0% O_2 in He, used without further purification.

Reaction rates of the SCR of NO and NO_2 and CH_4 combustion were measured in the temperature range of 450–600°C at a constant pressure of 1.5 atm (absolute). Separate experiments with GHSV in the range of 30,000 to 450,000 h^{-1} (STP) were conducted at each of the four temperatures, 450, 500, 550, and 600°C, to establish operation free from mass transfer limitation. The catalyst was

TABLE 1

Preparation of Ion-Exchanged Ag–, Ce–, and Ce–Ag–ZSM-5 Catalysts

Catalysts[a,b]	Si/Al[c]	Ce/Al[c]	Ag/Al[c]	Na/Al[c]	Charge balance[d]	Preparation conditions
Na–ZSM-5[e]	13.8	—	—	1.0	1.00	As received
Ag(18)–ZSM-5	12.9	—	0.18	0.75	0.93	Ag:0.002 *M*, once
Ag(31)–ZSM-5	13.2	—	0.31	0.65	0.96	Ag:0.01 *M*, once
Ag(54)–ZSM-5	12.8	—	0.54	0.33	0.87	Ag:0.01 *M*, once
Ag(77)–ZSM-5	12.4	—	0.77	0.08	0.85	Ag:0.01 *M*, twice
Ag(86)–ZSM-5	12.9	—	0.86	0.01	0.87	Ag:0.01 *M*, thrice
Ce(9)–ZSM-5	13.8	0.03	—	0.75	0.84	Ce:0.0003 *M*, once
Ce(21)–ZSM-5	14.2	0.07	—	0.73	0.94	Ce:0.01 *M*, once
Ce(42)–ZSM-5	13.8	0.14	—	0.62	1.04	Ce:0.01 *M*, twice
Ce(54)–ZSM-5	13.8	0.18	—	0.54	1.08	Ce:0.01 *M*, thrice
Ce(21)–Ag(11)–ZSM-5	12.8	0.07	0.11	0.60	0.92	Ce:0.01 *M*, once; Ag:0.001 *M*, once
Ce(21)–Ag(22)–ZSM-5	13.4	0.07	0.22	0.46	0.89	Ce:0.01 *M*, once; Ag:0.003 *M*, once
Ce(21)–Ag(42)–ZSM-5	11.7	0.07	0.42	0.33	0.99	Ce:0.01 *M*, once; Ag:0.006 *M*, once
Ce(24)–Ag(61)–ZSM-5	13.8	0.08	0.61	0.20	1.05	Ce:0.01 *M*, once; Ag:0.01 *M*, once
Ce(24)–Ag(78)–ZSM-5	14.0	0.08	0.78	0.01	1.03	Ce:0.01 *M*, once; Ag:0.01 *M*, twice
Ce(21)–Ag(80)–ZSM-5	13.8	0.07	0.80	0.00	1.01	Ce:0.01 *M*, once; Ag:0.01 *M*, thrice
Ce(9)–Ag(72)–ZSM-5	13.7	0.03	0.72	0.03	0.84	Ce:0.0003 *M*, once; Ag:0.01 *M*, twice
Ce(39)–Ag(75)–ZSM-5	11.7	0.13	0.75	0.00	1.14	Ce:0.01 *M*, twice; Ag:0.01 *M*, thrice
Ce(54)–Ag(67)–ZSM-5	13.2	0.18	0.67	0.00	1.21	Ce:0.01 *M*, thrice; Ag:0.01 *M*, thrice

[a] Each Ce ion exchange was performed at 80°C for 2 h with an aqueous solution of $Ce(NO_3)_3 \cdot 6H_2O$.
[b] Each Ag ion exchange was performed at room temperature in the dark for 24 h with an aqueous solution of $AgNO_3$.
[c] Si, Al, Ce, Ag, and Na contents were measured by ICP.
[d] Charge balance was calculated as (3Ce + Ag + Na)/Al. The calculated value is an upper bound for ion exchange.
[e] Na–ZSM-5 was supplied by the Davison Chemical Division, W.R. Grace & Co. Lot #: SMR 5-5829-0994, Si/Al = 13.8.

in fine powder form (<53 μm in size). Samples of 0.025–0.05 g and flow rates of 50–200 cc/min (GHSV = 30,000–180,000 h^{-1}, STP) were used in the measurements. Prior to each experiment, the catalyst was pretreated in helium at 500°C for 2 h. After cooling to room temperature, the reactant gas mixture was switched in and the temperature was raised to each preset point at a rate of 10°C/min. At each temperature, steady-state data were collected. Each test was run at a set temperature for 1.5 h after steady state was reached. The molar flow rates of N_2 produced and CH_4 consumed during reaction were used to calculate the conversion of NO to N_2 and CH_4 to CO_2. Under all test conditions reported here, CO was not detected in the product gases. Steady-state catalyst weight-based rates of NO reduction to N_2 and CH_4 oxidation were calculated as

$$\text{Rate of NO reduction to } N_2 = \frac{F_{NO} \times X_{NO}}{W} \text{ (mol/g/s)}$$

$$\text{Rate of } CH_4 \text{ oxidation} = \frac{F_{CH_4} \times X_{CH_4}}{W} \text{ (mol/g/s)},$$

where F_{NO} and F_{CH_4} are inlet molar flow rates of NO and CH_4, respectively; X_{NO} and X_{CH_4} the conversions of NO to N_2 and CH_4 to CO_2; and W the weight of catalyst loaded. The rate of NO reduction to N_2 (based on N_2 production) was used rather than the overall rate of NO consumption to avoid any errors by the potential gas-phase conversion of unreacted NO with oxygen to form NO_2 downstream of the reactor.

The kinetic measurements presented in this paper were not converted to turnover frequency (TOF) because in the silver-exchanged zeolite, we could not use chemisorption to characterize the silver. Reduction by hydrogen followed by oxygen chemisorption could change the dispersion of silver ions, but it would also be obscured by the contribution from cerium reduction ($Ce^{4+} \rightarrow Ce^{3+}$). As will be discussed later in the paper, HRTEM has identified that a fraction of silver exists in nanoparticle and cluster forms. The same is true for cerium, which is predominantly on the surface in fine oxide particle form (1–3 nm). Thus, it would be futile to try to separate the silver from the cerium phases by HRTEM/EDS and estimate the fraction of metallic silver at different silver loadings in Ce–Ag–ZSM-5 samples.

The catalyst selectivity is defined here with respect to methane as the rate of N_2 produced to the rate of total CH_4 consumed according to the following SCR reaction stoichiometry,

$$2NO + CH_4 + O_2 = N_2 + CO_2 + 2H_2O, \qquad \text{[I]}$$

and CH_4 oxidation by oxygen (combustion),

$$CH_4 + 2O_2 = CO_2 + 2H_2O. \qquad \text{[II]}$$

For the measurements of NO oxidation to NO_2, a 0.2-g sample and a flow rate of 50 cc/min (STP) were used. NO_2

was measured by a chemiluminescence NO/NO_x analyzer (Thermo Electron, Model 141A).

Catalyst Characterization

Selected fresh and reaction-aged catalyst samples were characterized by STEM/EDS, HRTEM/EDS, XPS, and UV-VIS DRS. The fresh samples were air-calcined at 500°C for 2 h. Aged samples were exposed to a gas mixture of 0.5% NO, 0.5% CH_4, 2.5% O_2, bal. He at 500°C for 24 h.

A VG HB603 scanning transmission electron microscope (STEM) equipped with an energy dispersive X-ray spectrometer (EDS) was used to study elemental distribution in the catalyst samples. The samples were supported on a 200 mesh copper grid in the STEM chamber without coating. The distribution of Ag, Ce, Si, Al, and O in the catalyst samples was obtained simultaneously with a spot size of 0.5 nm by 1 nm and a magnification of 5×10^5.

A JEOL 2010 high resolution transmission electron microscope (HRTEM) operated at 200 kV was used to study the morphology of catalyst samples. The TEM had an ultimate point-to-point resolution of 0.19 nm and was equipped with EDS for elemental analysis of selected sample areas. Catalyst samples were coated with carbon and supported on a 200 mesh copper grid in the TEM chamber.

A Perkin–Elmer Model 5100 X-ray photoelectron spectrometer (XPS) with 2-mm spatial resolution was used to determine metal ratios on the surface of catalyst samples. The Al K_α anode X-ray source was operated at 300 W. A layer of catalyst sample in powder form was pressed on a copper adhesive tape mounted on a sample holder. The sample was then introduced into the XPS vacuum chamber. The base pressure of the vacuum chamber was below 5×10^{-8} Torr. Each sample was exposed to the X-ray beam for about 40 min for data acquisition. Atomic ratios of silver and cerium to silicon in the surface region of the zeolite crystal were determined based on the core level spectra of Ag, Ce, and Si.

UV-visible diffuse reflectance (UV-VIS DR) spectra of Ce–, Ag–, and Ce–Ag–ZSM-5 were taken in a HP 8452A diode array spectrometer coupled with a Harrick diffuse reflectance attachment and a reaction chamber which could be heated up to 600°C. The spectra were recorded in the range of 180–820 nm with a resolution of 2 nm. High purity MgO (99.998%, Johnson Matthey) was used as reference material. *In situ* reduction and oxidation experiments were performed with 10% H_2–He and 20% O_2–He gas mixtures, respectively, at a flow rate of 20 cc/min (STP).

RESULTS

SCR of NO by CH_4

Activity studies. In a previous paper (19), we reported a significant promotion effect of cerium on Ag–ZSM-5 for the SCR of NO by CH_4 in the presence of excess oxygen. An 80% conversion of NO to N_2 was obtained over a Ce–Ag–ZSM-5 catalyst in a gas mixture of 0.5% NO, 0.5% CH_4, 2.5% O_2, bal. He, at a space velocity of 7500 h^{-1} (STP) at 500°C. However, only 20–25% conversion of NO to N_2 was measured over each of the Ag–ZSM-5 and Ce–ZSM-5 materials with equivalent metal loading at the same conditions. We found that 20–30% Ce^{3+} exchange (1–1.5 wt%) gave the maximum promotion effect, while the conversion of NO to N_2 increased linearly with Ag loading up to ~60% exchange level.

In the present work, the promotion effect was further examined in terms of NO reduction rate and CH_4 oxidation rate over the single-metal-loaded zeolite, Ag–ZSM-5 and Ce–ZSM-5, and the bi-metal Ce–Ag–ZSM-5 at the four temperatures of 450, 500, 550, and 600°C. Rate measurements over these three catalysts are shown in Table 2. Also listed in Table 2 is the catalyst selectivity. The two Ce-containing samples had approximately the same cerium ion exchange level of 21–24%, which corresponds to 1–1.2 wt% cerium. The Ag^+ ion exchange level was 78 and 77% (corresponding to ~8.5 wt% silver) in the promoted and unpromoted samples, respectively.

As shown in Table 2, the rate of NO reduction to N_2 increased with temperature over all three types of catalysts. No bend-over was observed over the temperature range from 450 to 600°C. Among the three catalysts, Ce(21)–ZSM-5 showed the lowest activity for the SCR reaction. The rate of NO reduction to N_2 over Ce(21)–ZSM-5 was three

TABLE 2

SCR Reaction Rates[a,b] and Catalyst Selectivity[c]

	NO to N_2				CH_4 to CO_2				Selectivity			
Temperature (°C)	450	500	550	600	450	500	550	600	450	500	550	600
Ce(21)–Z	0.08	0.12	0.17	0.23	0.05	0.08	0.18	0.37	0.85	0.72	0.48	0.31
Ag(77)–Z	0.24	0.50	1.16	1.91	0.30	0.44	3.43	5.07	0.40	0.56	0.17	0.18
Ce(24)–Ag(78)-Z	0.38	1.00	2.59	4.38	0.21	0.59	2.94	7.09	0.91	0.84	0.44	0.31

[a] mmol NO or CH_4/g catalyst · s × 10^3.

[b] Measurements were performed with a gas mixture of 0.5% NO-0.5% CH_4-2.5% O_2-bal. He, at SV = 30,000–180,000 h^{-1}.

[c] The catalyst selectivity is defined as the ratio of the rate of N_2 produced/rate of CH_4 consumed according to reactions I and II.

to eight times less than that over Ag(77)–ZSM-5 and 5–19 times less than that over Ce(24)–Ag(78)–ZSM-5. This indicates that Ce–ZSM-5 is a poor catalyst for the SCR of NO with CH_4. A higher NO reduction rate was obtained over the Ag(77)–ZSM-5 sample, which varied from 0.24×10^{-3} to 1.91×10^{-3} mmol/g·s in the temperature range of 450–600°C. The highest NO reduction rate was measured over the bi-metal Ce(24)–Ag(78)–ZSM-5. As shown in Table 2, this was 1.5–2.5 times higher than that over Ag(77)–ZSM-5. Thus, incorporation of a small amount of cerium into Ag–ZSM-5 promoted the activity of the latter for the SCR reaction.

The promotion effect is further manifested by the different methane oxidation rate and different selectivity over these catalysts as shown in Table 2. The CH_4 oxidation rate shown in this table is for the overall CH_4 oxidation by both ($NO + O_2$) in reaction I and O_2 in reaction II. Similar to its low catalytic activity for the SCR reaction, Ce(21)–ZSM-5 also had the lowest CH_4 oxidation rate among the three catalyst types. The data in Table 2 indicate that Ce–ZSM-5 is practically inactive for CH_4 combustion. On the other hand, Ag(77)–ZSM-5 showed almost the same rate of CH_4 oxidation as Ce(24)–Ag(78)–ZSM-5, although the activity of the former for converting NO to N_2 was lower. As a result, the selectivity of Ag(77)–ZSM-5 was the lowest among the three catalysts, indicating that Ag(77)–ZSM-5 was more active for CH_4 combustion than for the SCR reaction. For Ce(24)–Ag(78)–ZSM-5, although its SCR rate was increased by a factor of 1.5–2.5 upon the incorporation of Ce compared to that of Ag(77)–ZSM-5, its CH_4 oxidation rate remained essentially the same (except at 600°C). Therefore, the presence of cerium also enhanced the CH_4 selectivity of Ag–ZSM-5 significantly as shown in Table 2.

Effect of Ag loading. The dependence of the catalytic activity of Ce–Ag–ZSM-5 on Ag loading was studied over a set of samples with a fixed Ce exchange level of 21–24% and various Ag exchange levels from 11 to 85%. Figures 1a and 1b show the rate of NO reduction to N_2 and rate of overall CH_4 oxidation, respectively, at the four temperatures of 450, 500, 550, and 600°C.

As shown in Fig. 1a, at a given temperature, the rate of NO reduction increased linearly with Ag loading up to approximately Ag/Al = 0.6 (atomic ratio), suggesting that within the range of Ag/Al = 0–0.6, Ag ions incorporated into the ZSM-5 zeolite were approximately equivalent to each other in terms of their effectiveness to convert NO to N_2. However, with further increase of Ag loading from Ag/Al = 0.6 to 0.85, the rate of NO reduction leveled off, especially at the high temperatures of 550 and 600°C. The dependence of CH_4 oxidation rate on Ag/Al is very different as shown in Fig. 1b. At 450 and 500°C, CH_4 oxidation by O_2 contributed very little to the overall CH_4 oxidation as indicated by the very low CH_4 oxidation rate. At these two temperatures, CH_4 was primarily consumed by the SCR reaction, resulting in the high selectivity of Ce–Ag–ZSM-5 at 450 and 500°C shown in Table 2. At 550 or 600°C, Fig. 1b shows that an initial slow increase of CH_4 oxidation rate in the lower Ag/Al range was followed by a much faster increase at higher Ag/Al ratios, in contrast to what was observed in Fig. 1a, i.e. the leveling-off of the NO reduction rate at high Ag/Al ratios. These data clearly demonstrate that catalysts with higher silver loading are more active for CH_4 combustion.

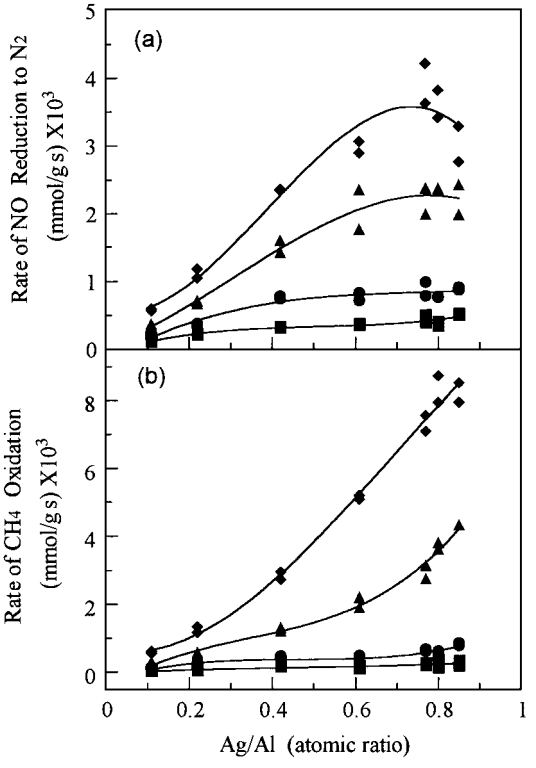

FIG. 1. Effect of Ag loading on the rate of (a) NO reduction to N_2 and (b) overall CH_4 oxidation in the SCR of NO by CH_4 over Ce–Ag–ZSM-5 catalysts. Ce exchange level = 21–24%. Feed gas: 0.5% NO–0.5% CH_4–2.5% O_2–bal. He. SV = 30,000–180,000 h^{-1}. Symbols: ■, 450°C; ●, 500°C; ▲, 550°C; ◆, 600°C.

Effect of Ce loading. The dependence of Ce–Ag–ZSM-5 activity on Ce loading is shown in Figs. 2a and 2b at a Ag ion exchange level of 67–80%. The Ce loading was varied from Ce/Al = 0 to 0.18. As shown in Fig. 2a, at each temperature tested, the rate of NO reduction to N_2 first increased with the Ce/Al ratio reaching a maximum at approximately Ce/Al = 0.1–0.13, which corresponds to ~1.5% cerium by weight. With further increase of Ce loading, the rate of NO reduction declined. Thus, a small amount of cerium (~1.5 wt% Ce) provided the maximum promotion of the SCR reaction.

The effect of cerium loading on the catalyst activity for CH_4 oxidation depends on the operating temperature. As shown in Fig. 2b, different profiles of CH_4 oxidation rate vs the Ce/Al atomic ratio were obtained at 450, 500, 550,

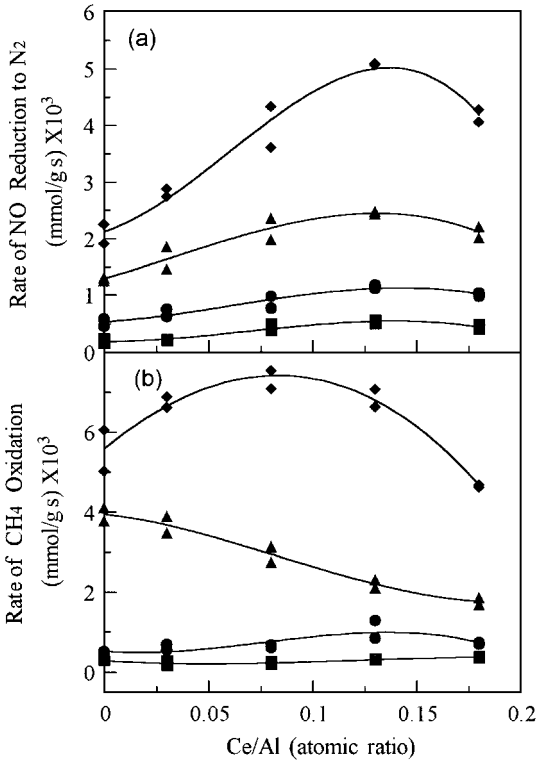

FIG. 2. Effect of Ce loading on the rate of (a) NO reduction to N_2 and (b) overall CH_4 oxidation in the SCR of NO by CH_4 over Ce–Ag–ZSM-5 catalysts. Ag exchange level = 67–80%. Feed gas: 0.5% NO–0.5% CH_4–2.5% O_2–bal. He. SV = 30,000–180,000 h^{-1}. Symbols: ■, 450°C; ●, 500°C; ▲, 550°C; ◆, 600°C.

and 600°C. At 450 and 500°C, the methane oxidation rate did not change much with the Ce/Al ratio. A monotonic decrease of methane oxidation rate with Ce/Al was obtained at 550°C, in contrast with the dependence of NO reduction rate on cerium loading at the same temperature shown in Fig. 2a. This suggests that incorporation of Ce in Ag–ZSM-5 suppressed the CH_4 oxidation by O_2, resulting in higher catalyst selectivity. At 600°C, a maximum CH_4 oxidation rate was obtained at Ce/Al = ~0.08. The initial increase of the CH_4 oxidation rate with cerium at Ce/Al < 0.08 was due to the fast increase of the rate of SCR reaction with cerium loading at 600°C as shown in Fig. 2a. Above Ce/Al > 0.08, the suppression effect of cerium and the drop of the SCR reaction rate took control, resulting in the bend-over of the CH_4 oxidation rate with cerium.

CH_4 Combustion

In separate tests, kinetic measurements of methane combustion were carried out over a series of Ce–ZSM-5, Ag–ZSM-5, and Ce–Ag–ZSM-5 catalysts with various Ag loadings using a feed gas mixture of 0.5% CH_4, 2.5% O_2, bal. He. Because of low CH_4 conversion, reliable values for the reaction rate could not be obtained over Ce–ZSM-5 at high space velocity (>30,000 h^{-1}) where the reaction was

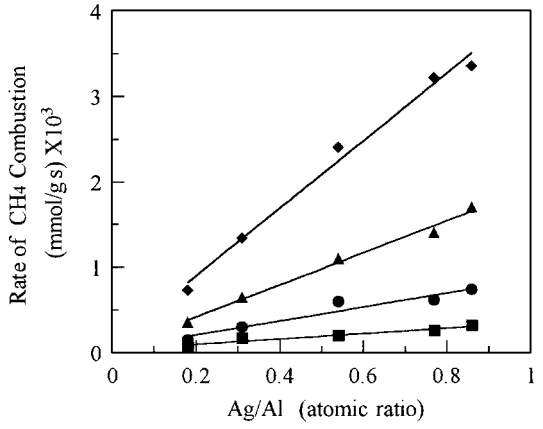

FIG. 3. Effect of Ag loading on the rate of CH_4 combustion over Ag–ZSM-5 catalysts. Feed gas: 0.5% CH_4–2.5% O_2–bal. He. SV = 30,000–120,000 h^{-1}. Symbols: ■, 450°C; ●, 500°C; ▲, 550°C; ◆, 600°C.

free of mass transfer limitations. However, CH_4 conversion data obtained at a GHSV of 7500 h^{-1} have shown that Ce–ZSM-5 is not an effective catalyst for CH_4 combustion (19). By contrast, Ag–ZSM-5 is active for this reaction, especially at high silver loadings. Light-off of the reaction occurred at about 450°C and complete conversion of CH_4 to CO_2 was measured at 600°C over Ag(77)–ZSM-5 (19).

The effect of Ag loading on the activity of unpromoted and Ce-promoted Ag–ZSM-5 catalysts for CH_4 combustion is shown in Fig. 3 and 4, respectively, in terms of the rate of CH_4 combustion vs the Ag/Al atomic ratio at four temperatures: 450, 500, 550, and 600°C. The corresponding values are also listed in Table 3. At each temperature, the rate of CH_4 combustion increased with the Ag/Al ratio over the entire silver loading range tested for both types of catalysts. However, over the unpromoted Ag–ZSM-5 (Fig. 3), a linear relationship between the rate of CH_4 combustion

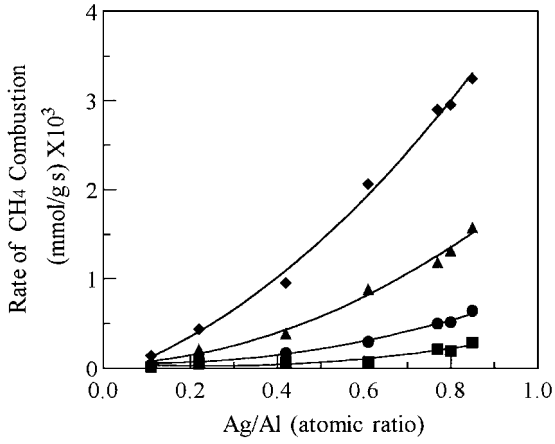

FIG. 4. Effect of Ag loading on the rate of CH_4 combustion over Ce–Ag–ZSM-5 catalysts. Ce exchange level = 21–24%. Feed gas: 0.5% CH_4–2.5% O_2–bal. He. SV = 30,000–120,000 h^{-1}. Symbols: ■, 450°C; ●, 500°C; ▲, 550°C; ◆, 600°C.

TABLE 3

Rate of CH_4 Oxidation in CH_4 Combustion Experiments[a,b]

Ag/Al	Temperature (°C) 450	500	550	600
		Ag–ZSM-5		
0.18	0.07	0.15	0.35	0.73
0.31	0.16	0.30	0.65	1.34
0.54	0.20	0.60	1.09	2.40
0.77	0.25	0.61	1.40	3.22
0.86	0.32	0.74	1.69	3.35
		Ce–Ag–ZSM-5[c]		
0.11	0.02	0.03	0.06	0.14
0.22	0.06	0.11	0.21	0.44
0.42	0.07	0.17	0.39	0.95
0.61	0.08	0.29	0.89	2.06
0.78	0.21	0.50	1.19	2.90
0.80	0.20	0.51	1.32	2.95
0.85	0.29	0.64	1.58	3.25

[a] In mmol/g · s × 10^3.

[b] Feed gas mixture was 0.5% CH_4, 2.5% O_2, bal. He at SV = 30,000–120,000 h^{-1}.

[c] The cerium loading was 21–24% in exchange level.

and Ag/Al ratio was obtained at each temperature, while over the promoted Ce–Ag–ZSM-5 (Fig. 4), a nonlinear correlation was found. By comparing the corresponding rate in Fig. 3 and that in Fig. 4 at a given Ag/Al ratio, it can be seen that at low Ag/Al ratios, the rate of CH_4 combustion over Ce–Ag–ZSM-5 was much lower than that over the unpromoted Ag–ZSM-5. As Ag/Al was increased, the rate of CH_4 combustion increased and approached that of the unpromoted samples. For example, at 600°C, the rate of CH_4 combustion over a Ce–Ag–ZSM-5 with Ag/Al = 0.2 was 0.40×10^{-3} mmol/g · s which was about one half of that over a Ag–ZSM-5 sample with the same Ag loading (0.75×10^{-3} mmol/g · s). However with Ag/Al = 0.85 at the same temperature, the rate of CH_4 combustion for the Ce–Ag–ZSM-5 and Ag–ZSM-5 samples was very close, i.e., 3.25×10^{-3} and 3.35×10^{-3} mmol/g · s, respectively. This is true at all four temperatures, as shown in Table 3, and demonstrates that the activity of Ce–Ag–ZSM-5 for CH_4 oxidation by O_2 is lower than that of Ag–ZSM-5 with the same silver loading. In other words, the presence of cerium in Ag–ZSM-5 suppressed the catalyst activity for the CH_4 combustion, especially at low Ag loadings, consistent with the data in Fig. 2b.

NO Oxidation to NO_2

In much of the HC-SCR literature, it has been pointed out that an important role of O_2 in the SCR reaction is to convert NO to NO_2 (3, 25–27). In a study of NO reduction by propane over Ce–ZSM-5 catalysts by Yokoyama *et al.* (25), Ce–ZSM-5 as well as bulk CeO_2 were reported active for the oxidation of NO to NO_2. Haneda *et al.* (28) have recently reported that the major function of Ag in a Ag/TiO_2–ZrO_2 catalyst for the SCR of NO with propene, 2-propanol, or acetone was to catalyze the reaction of NO_2 with the hydrocarbons. These studies suggest that a potential role of Ce in Ce–Ag–ZSM-5 is to catalyze the oxidation of NO to NO_2, while the reaction of NO_2 with CH_4 takes place on Ag sites. To examine this hypothesis, separate studies of oxidation of NO to NO_2 and SCR of NO_2 by CH_4 were carried out over Ag–ZSM-5, Ce–ZSM-5, and Ce–Ag–ZSM-5 catalysts.

The NO oxidation experiments were conducted with a feed gas mixture of 0.2% NO, 2.5% O_2, bal. He. The results are shown in Fig. 5 together with the data obtained with an empty reactor. The thermodynamic equilibrium conversions for NO to NO_2 are also shown in Fig. 5. At temperatures below 450°C, Ce(54)–ZSM-5 showed the same activity for converting NO to NO_2 as Ce(54)–Ag(67)–ZSM-5. Similar results were reported by Yokoyama *et al.* (25) over a Ce(15)–ZSM-5 catalyst. The conversion of NO to NO_2 over the Ag(77)–ZSM-5 sample was the lowest of the three catalysts shown in Fig. 5, suggesting that Ce sites are more active than Ag sites for the oxidation of NO to NO_2 at low temperatures. At temperatures above 500°C, the reaction is limited by equilibrium and the gas-phase concentration of NO_2 is very low over all the catalysts, as shown in Fig. 5.

SCR of NO_2 by CH_4

The rate of NO_2 reduction by CH_4 was measured in both the presence and the absence of oxygen over Ag(77)–ZSM-5 and Ce(24)–Ag(78)–ZSM-5 using a feed gas stream of 0.2% NO_2, 0.5% CH_4, 2.5 or 0% O_2, bal. He at GHSV = 30,000–180,000 h^{-1}. The results are shown in Fig. 6 in terms of the rate of NO_2 reduction to N_2 vs temperature. With

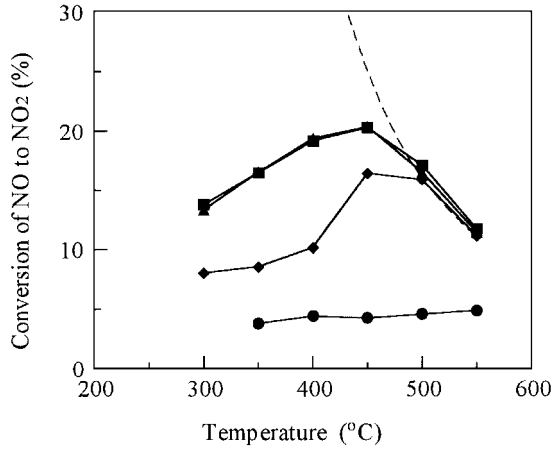

FIG. 5. Oxidation of NO to NO_2 by O_2. Feed gas: 0.2% NO–2.5% O_2–bal. He. Sample weight = 0.2 g, flow rate = 50 cc/min. Symbols: ●, Empty reactor; ■, Ce(54)–ZSM-5; ◆, Ag(77)–ZSM-5; ▲, Ce(54)–Ag(67)–ZSM-5; dashed line, equilibrium.

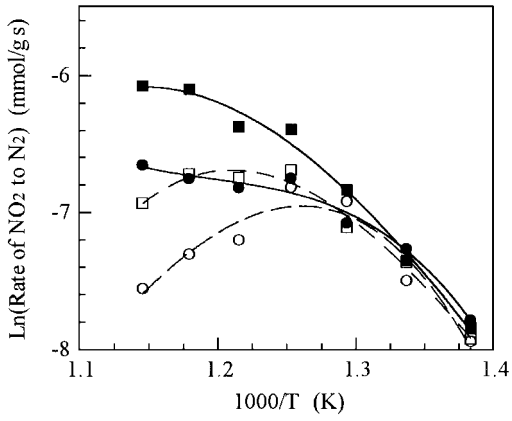

FIG. 6. Rate of NO_2 reduction to N_2 in the SCR of NO_2 by CH_4 in the presence and absence of O_2. Feed gas: 0.2% NO_2–0.5% CH_4–2.5% O_2–bal. He. (solid lines), 0.2% NO_2–0.5% CH_4–bal. He (dashed lines). SV = 30,000–180,000 h^{-1}. Symbols: ● and ○, Ag(77)–ZSM-5; ■ and □, Ce(24)–Ag(78)–ZSM-5.

NO_2 in the feed gas mixture, the unpromoted Ag(77)–ZSM-5 sample showed the same rate of NO_2 reduction to N_2 as the Ce-promoted Ce(24)–Ag(78)–ZSM-5 sample in the low temperature range (<500°C), regardless of the presence or absence of O_2. This result agrees well with our earlier report that the conversion of NO_2 to N_2 over a Ag–ZSM-5 catalyst became identical to that of a Ce–Ag–ZSM-5 catalyst upon substitution of NO with NO_2 when the temperature was lower than 500°C (19). At temperatures above 500°C, Fig. 6 shows a significant difference in activity between the Ag(77)–ZSM-5 and Ce(24)–Ag(78)-ZSM-5 samples for NO_2 reduction. The rate of NO_2 reduction to N_2 over the Ag(77)–ZSM-5 sample was much lower, and it either leveled off earlier in the presence of oxygen (solid lines) or bent-over earlier in the absence of oxygen (dashed lines) compared to the rate over Ce(24)–Ag(78)–ZSM-5 at the same conditions.

Catalyst Characterization

STEM/EDS and HRTEM/EDS. The morphology and the elemental distributions of Si, Al, Ag, and Ce in fresh and aged Ag–ZSM-5 and Ce–Ag–ZSM-5 samples were examined by STEM/EDS and HRTEM/EDS. Figures 7a and 7b show the elemental mappings taken over two low Ag-content samples: Ag(54)–ZSM-5 and Ce(21)–Ag(42)–ZSM-5 after calcination. The annular dark form (ADF) images in the pictures show the area of the samples on which elemental mappings were taken. Magnification of each elemental mapping is 5×10^5. In both the unpromoted Ag(54)–ZSM-5 and the promoted Ce(21)–Ag(42)–ZSM-5 solids, uniform distribution of Ag was observed at this level of Ag exchange. The Ag distribution closely matches the Al distribution in the two samples, showing a strong association of Ag with framework Al. This indicates that at low Ag exchange levels (<~50%), Ag is highly dispersed in both types of materials in the as-prepared form (calcined in air for 2 h at 500°C).

As Ag loading was increased, Ag dispersion decreased as shown in Figs. 7c and 7d for the Ag(77)–ZSM-5 and the Ce(24)–Ag(78)–ZSM-5 samples. Compared with the Ag dispersion in Figs. 7a and 7b, aggregation of Ag (clusters) is observed in these two high Ag-content samples, although the distribution of Al is still uniform. However, in the presence of cerium, the extent of Ag clustering was lower in Ce(24)–Ag(78)–ZSM-5 (Fig. 7d) than in Ag(77)–ZSM-5 (Fig. 7c). This suggests that another function of cerium in Ce–Ag–ZSM-5 is to keep silver better dispersed. The same function of Ce has been reported for the Ce–Cu–ZSM-5 system (29).

The above observations were confirmed by the HRTEM/EDS analysis, as shown in Figs. 8a and 8b for the fresh (as-prepared) Ag(77)–ZSM-5 and Ce(24)–Ag(78)–ZSM-5 samples, respectively. In Fig. 8a, particles of size 5–30 nm are observed. Strong surface agglomeration is clearly seen in this sample. On the promoted Ce(24)–Ag(78)–ZSM-5 sample (Fig. 8b), particles in the size range of ~8–12 nm as well as highly dispersed clusters of 1- to 3-nm size are observed. X-ray emission analysis performed on the large particles identified them as metallic silver. In the areas where large silver particles were absent, X-ray emission corresponding to silver and cerium was obtained in addition to Si, Al, and O. In this case, the silver emission was due to Ag^+ ions embedded in the zeolite. As will be shown below, XPS identified that most of the cerium was concentrated on the surface of the zeolite particles. Thus, the 1- to 3-nm clusters located on the surface of the zeolite are Ce species, most likely in oxidized form. Clearly, in the promoted sample, the number density of Ag particles was much lower (Figs. 8a and 8b).

After an aging test with 0.5% NO, 0.5% CH_4, 2.5% O_2, bal. He at 500°C for 24 h, Ag were found aggregates in the Ag(77)–ZSM-5 sample. As shown in Fig. 9a, the signal intensity of Al (white dots in Al mapping) at the right edge of the sample is slightly weaker than that in other parts of the sample; however, the Ag signal at the same location is much stronger. Thus, aggregation of silver due to reaction occurred in this sample. However, after aging at the same conditions, the dispersion of Ag in the Ce(24)–Ag(78)–ZSM-5 sample (Fig. 9b) is essentially the same as that of the fresh one (Fig. 8d), suggesting little structural change.

The state of Ce remained similar in the fresh and aged Ce–Ag–ZSM-5 catalysts as can be seen in Figs. 7b, 7d, and 9b. Well-dispersed clusters of cerium phases are observed in all Ce-containing samples although the Ce loading was low (~1 wt%). No bulk CeO_2 reflections were found by X-ray diffraction analysis of these samples.

XPS. The atomic ratios of Ag and Ce to Si in the surface region of the fresh and aged Ag(77)–ZSM-5 and Ce(24)–Ag(78)–ZSM-5 samples were measured by XPS.

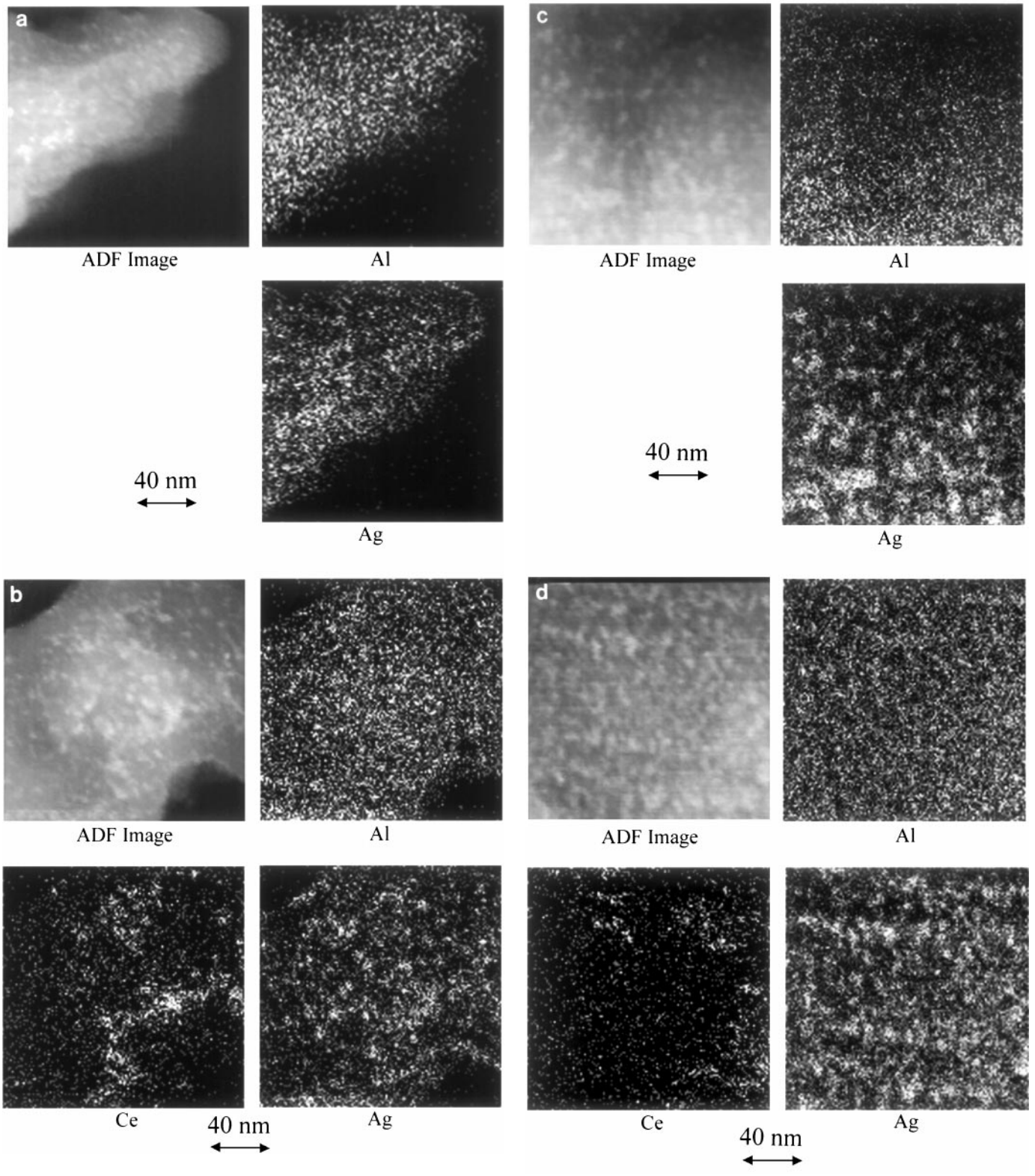

FIG. 7. STEM/EDS elemental mappings of fresh (a) Ag(54)–ZSM-5, (b) Ce(21)–Ag(42)–ZSM-5, (c) Ag(77)–ZSM-5, and (d) Ce(24)–Ag(78)–ZSM-5.

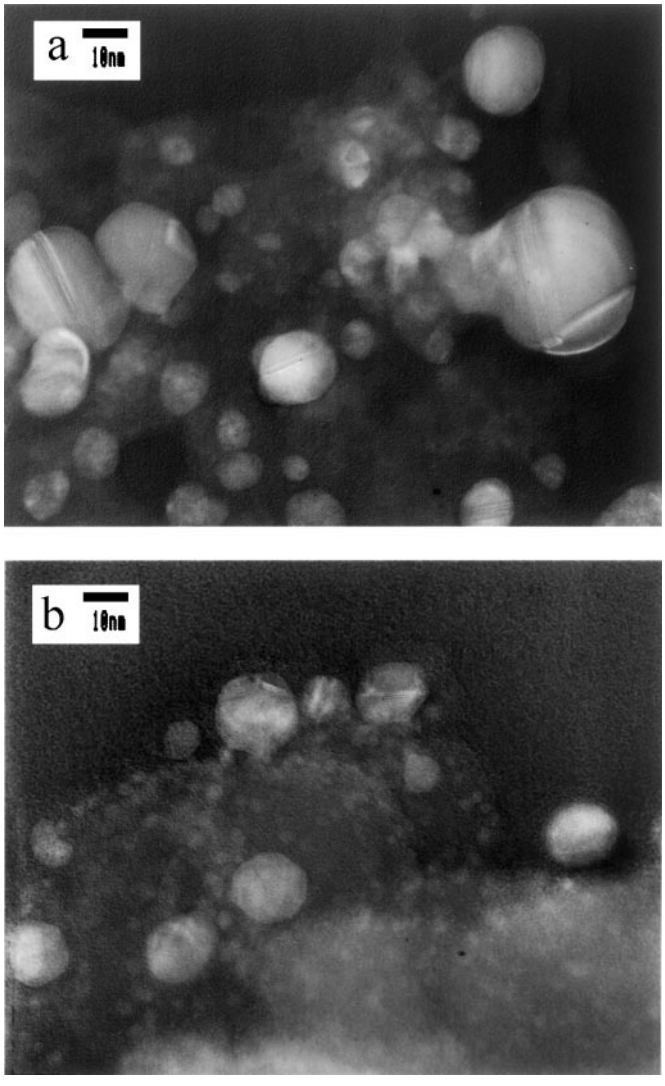

FIG. 8. HRTEM images of fresh (a) Ag(77)–ZSM-5 and (b) Ce(24)–Ag(78)–ZSM-5.

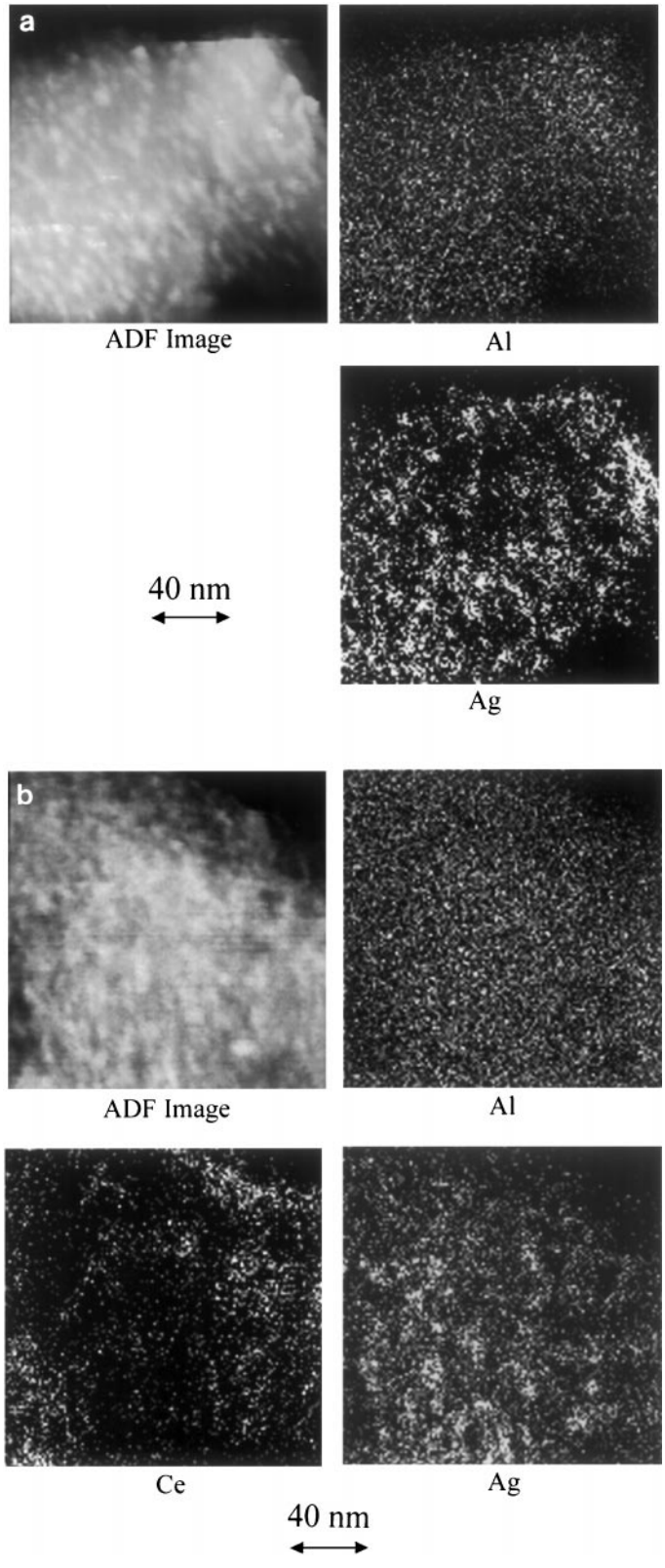

FIG. 9. STEM/EDS elemental mappings of reaction-aged (a) Ag(77)–ZSM-5 and (b) Ce(24)–Ag(78)–ZSM-5. Reaction-aging was performed in 0.5% NO–0.5% CH_4–2.5% O_2–bal. He at 500°C for 24 h.

The surface atomic ratios of Ag and Ce to Si are shown in Fig. 10 along with the bulk ratios measured by ICP for comparison. Clearly, in the unpromoted Ag(77)–ZSM-5 sample, the surface Ag/Si ratio was higher than the bulk, i.e., 0.09 vs 0.058, consistent with the STEM/EDS Ag mapping (Fig. 7c) and HRTEM image (Fig. 8a) of the same material, in which silver particles were observed. After aging, the surface Ag concentration was further increased, i.e., Ag/Si = 0.107. However, for the fresh and aged Ce(24)–Ag(78)–ZSM-5 samples, the surface Ag/Si ratios were 0.065 and 0.058, respectively. These values are both close to the bulk Ag/Si ratio of 0.058, implying that Ag was better dispersed in the presence of cerium. The surface ratios of Ce/Si in the Ce(24)–Ag(78)–ZSM-5 sample before and after aging (∼0.12–0.13) were significantly higher than the corresponding bulk value measured by ICP (0.006), indicating

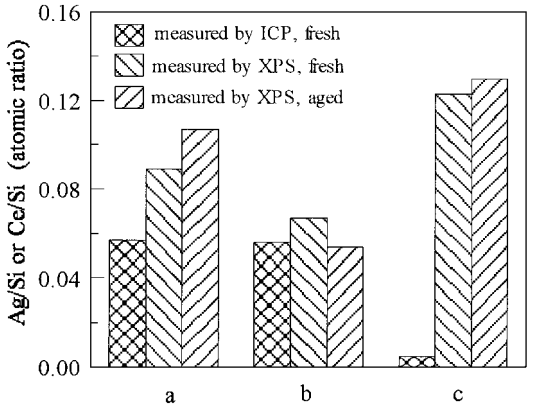

FIG. 10. Comparison of surface (by XPS) and bulk (by ICP) Ce and Ag concentrations in fresh and reaction-aged catalysts. (a) Ag/Si ratio in Ag(77)–ZSM-5, (b) Ag/Si ratio in Ce(24)–Ag(78)–ZSM-5, and (c) Ce/Si ratio in Ce(24)–Ag(78)–ZSM-5. Reaction-aging was performed in 0.5% NO–0.5% CH_4–2.5% O_2–bal. He at 500°C for 24 h.

surface enrichment of cerium, in agreement with the STEM/EDS and HRTEM analyses in Figs. 7d, 8b, and 9b.

UV-VIS DRS. UV-VIS DRS was used to examine the oxidation states and electronic transition of Ce and Ag reduction–oxidation of the catalysts. Figure 11 shows the *in situ* UV-VIS DR spectra of Ag(77)–ZSM-5 during successive reduction and oxidation treatments at various temperatures. The spectrum of the parent Na–ZSM-5 has been subtracted from these spectra. As can be seen in this figure, at room temperature (25°C) in air, the UV-VIS DR spectrum of Ag(77)–ZSM-5 displays three overlapped bands at 196, 212, and 222 nm, a small peak at around 300 nm, and a broad peak at 420 nm. A similar spectrum was obtained in pure He (curve 2 in Fig. 11). The three overlapped bands have been assigned to the $4d^{10} \rightarrow 4d^9 5s^1$ electronic transition of isolated Ag^+ ions in the zeolite matrix (30–33). The broad band at 420 nm is characteristic of metallic silver particles and aggregates with a size of several nanometers or greater (33, 34). Upon reduction by H_2 at 300 and 500°C, this band grew appreciably, and the band at 300 nm evolved to a distinct doublet peak (295 and 315 nm) with a shoulder at 335 nm, indicating that absorption at these wavelengths was due to the electronic transition of reduced Ag species. These species may be oligometric Ag_n clusters (absorption band at 285–345 nm) (34, 35) or a film-like (bulk Ag) structure at 310–315 nm (33, 36), also of a relatively large size as evidenced by the fact that they could not be oxidized fully at 300°C (37). At temperatures above 300°C, the bands at 295, 315, and 335 nm decayed in the presence of oxygen and, simultaneously, bands at 258 developed (curves 4, 6, 7 in Fig. 11). The latter may be assigned to oxidized $Ag_n^{\delta+}$ clusters (31, 34).

UV-VIS DR spectra for various air-calcined Ce–ZSM-5, Ag–ZSM-5, and Ce–Ag–ZSM-5 samples are shown in Figs. 12a–12c, respectively. These spectra were taken in air at room temperature. Ce–ZSM-5 samples show a well-resolved peak at 294 nm (Fig. 12a). Two shoulders at 260 and 210 nm can also be seen, especially at low Ce loadings, i.e., Ce(9)–ZSM-5 and Ce(21)–ZSM-5. But these two bands were very weak in the high cerium-containing samples. The bands at 260 and 210 nm are due to the 4*f*–5*d* interconfiguration transitions of Ce^{3+} species (38, 39), while the band at 294 nm is attributed to the $Ce^{4+} \leftarrow O^{2-}$ charge transfer of CeO_2 clusters of several nanometers in size (39, 40). Thus, a mixture of cerium in 3+ and 4+ states co-existed in Ce–ZSM-5. The intensity of the band at 294 nm increased with Ce exchange level while the two bands at 260 and 210 nm disappeared at high Ce loadings, suggesting the presence of CeO_2 predominantly in high cerium-containing samples. In Ce–Ag–ZSM-5 catalysts (Fig. 12c), the two bands for Ce^{3+} could not be distinguished because of the overlapping of cerium and silver spectra. Only the 294-nm band for CeO_2 clusters can be seen, whose intensity increased with cerium loading.

All Ag–ZSM-5 catalysts displayed similar absorption spectra as shown in Fig. 12b: three overlapping peaks at 196, 212, and 222 nm, a small peak at 300 nm, and a broad peak at 420 nm. The band at 300 nm was present in all samples, while the broad band at 420 nm grew with Ag exchange,

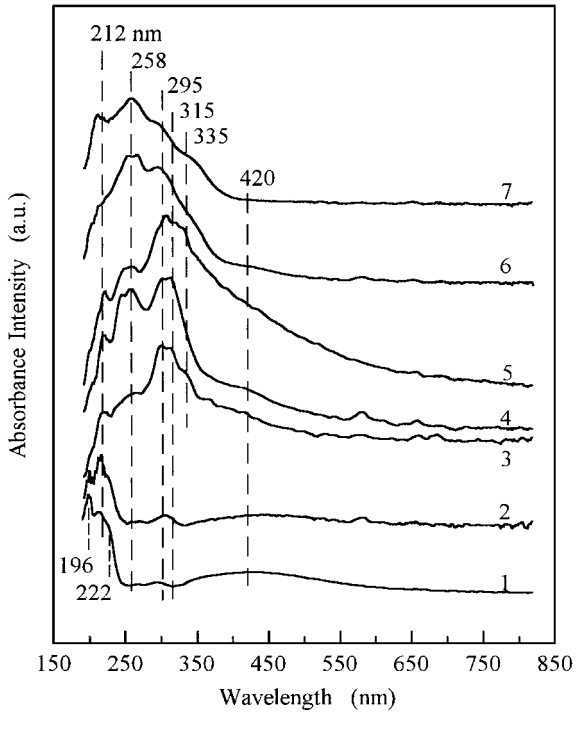

FIG. 11. *In situ* UV-VIS DR spectra in reduction and oxidation of Ag(77)–ZSM-5. (1) 25°C in air; (2) 25°C in He; (3) 300°C in H_2; (4) 300°C in O_2; (5) 500°C in H_2; (6) 500°C O_2; (7) 600°C in O_2. Reduction gas was 10% H_2 in He at a flow rate of 20 ml/min. Oxidation gas was 20% O_2 in He at a flow rate of 20 ml/min.

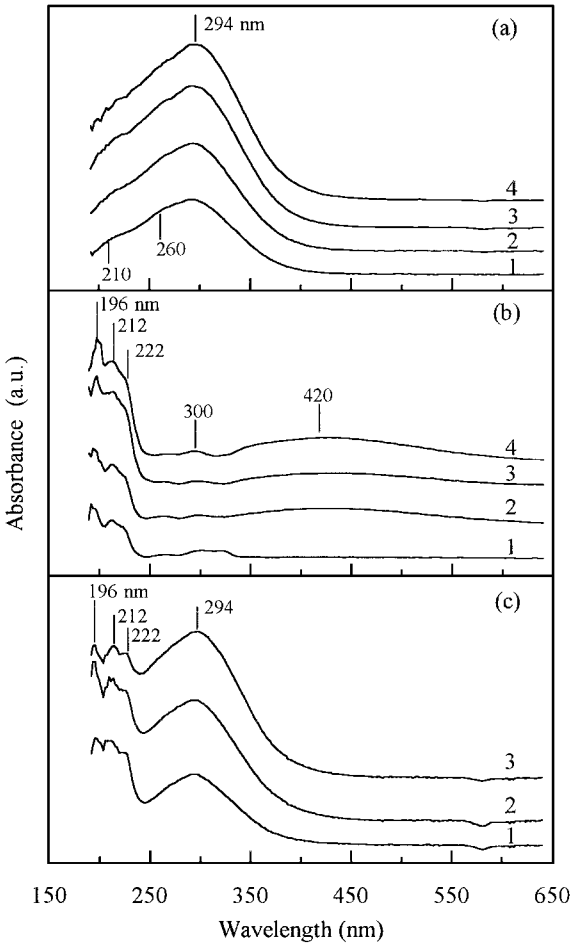

FIG. 12. UV-VIS DR spectra of fresh Ce–, Ag–, and Ce–Ag–ZSM-5 samples. (a) 1-Ce(9), 2-Ce(24), 3-Ce(42), 4-Ce(54)-ZSM-5; (b) 1-Ag(18), 2-Ag(31), 3-Ag(54), 4-Ag(77)–ZSM-5; (c) 1-Ce(9)–Ag(72), 2-Ce(24)–Ag(78), 3-Ce(54)–Ag(67)–ZSM-5. All spectra were taken in air at room temperature.

indicating that more metallic silver particles were formed as Ag loading was increased. Therefore, in the fresh Ag–ZSM-5 samples, silver existed as highly dispersed Ag^+ ions, Ag_n clusters, and metallic silver particles. In the presence of Ce, the peak at 420 nm disappeared as shown in Fig. 12c. The absence of this band in the Ce–Ag–ZSM-5 suggests that the interaction of Ce and Ag inhibits the formation of large metallic silver particles. This is consistent with our observation of color changes with these materials. A gradation from white to gray color from the Ag(18)– to Ag(77)–ZSM-5 samples was observed, while all Ce–Ag–ZSM-5 samples were white.

DISCUSSION

In the presence of excess oxygen, reactions I and II may take place simultaneously. The CH_4 selectivity of a catalyst may strongly depend on the structure of the catalyst as has been demonstrated for Pd–HZSM-5 (41, 42). Highly dispersed Pd^{2+} ions favor the SCR reaction, while PdO_x particles catalyze the CH_4 oxidation by O_2. In view of the findings of the present work, the sites catalyzing the SCR reaction and CH_4 oxidation by O_2 in Ce–Ag–ZSM-5 are different. Thus, structural effects are also present in this system. The evidence for this and the role of cerium in modulating catalyst selectivity are discussed below.

Catalyst Preparation and Structure

During sample preparation, we found that Ag^+ ions could be easily exchanged into the zeolite matrix to high exchange levels, but for Ce^{3+}, high exchange levels were difficult to achieve. Protonation of some exchange sites might also have occurred during the exchange of either Ce^{3+} or Ag^+ ions as indicated by the charge imbalance in Table 1 and by the presence of clusters of cerium oxide and silver particles on the zeolite surface (Figs. 7–10). However, the presence of Brønsted acid sites is not important for the SCR activity of Ag–ZSM-5 as we found in separate experiments where silver was exchanged in HZSM-5 rather than the Na–ZSM-5 zeolite (18, 19). This is in contrast to the case of Pd-exchanged ZSM-5 where protons have been reported as essential for the SCR reaction, while Na has a deleterious effect (10, 41).

The oxidation state and dispersion of both Ce and Ag in the zeolite strongly depend on their exchange levels. At low exchange levels (<50–60%), Ag was well dispersed in both the promoted and unpromoted samples as shown in Figs. 7a and 7b. The strong association of Ag^+ ions with the framework Al in these two figures implies that most Ag^+ ions exchanged the Na^+ ions on the AlO_2^- sites of the zeolite. In Table 4, the increase of Ag^+ or Ce^{3+} exchange level (columns C and E, respectively) is compared with the loss of Na^+ ions (column G) during the ion exchange step for Ag–ZSM-5 and Ce–ZSM-5, based on ICP measurements. The number of Na^+ ions (column G) being replaced is greater than the corresponding number of Ag^+ ions (column C) exchanged into the zeolite at low Ag exchange levels, indicating both one to one exchange of Ag^+ for Na^+ as well as protonation of some exchange sites. As Ag loading was increased, aggregation of Ag occurred in both the promoted and unpromoted Ag–ZSM-5 as evidenced by the formation of Ag particles in Figs. 7c, 7d, and 8. These particles are metallic in nature as indicated by the HRTEM/EDS and UV-VIS DRS analyses, Figs. 8 and 12, respectively. Migration of silver complexes to the surface followed by dehydration and agglomeration during calcination may contribute to the formation of metallic silver particles (31).

The UV-VIS DR spectra in Figs. 12a and 12c show that cerium in the Ce–ZSM-5 and Ce–Ag–ZSM-5 catalysts exists both in the 3+ and 4+ oxidation states. The latter is the dominant state for catalysts with high Ce loading. These results are consistent with those reported by Zhang *et al.* (29), who used luminescence to identify the presence of

TABLE 4

Comparison of the Increments of Ag and Ce Ion-Exchange Levels with the Loss of Na Ions during Ion-Exchange[a]

A Catalysts	B Ag/Al	C[b] ΔAg/Al	D Ce/Al	E[c] Δ(3 × Ce/Al)	F Na/Al	G[d] −ΔNa/Al
Na–ZSM-5	0.0		—	—	1.0	
		0.18				0.25
Ag(18)–ZSM-5	0.18		—	—	0.75	
		0.13				0.10
Ag(31)–ZSM-5	0.31		—	—	0.65	
		0.23				0.32
Ag(54)–ZSM-5	0.54		—	—	0.33	
		0.23				0.25
Ag(77)–ZSM-5	0.77		—	—	0.08	
		0.09				0.07
Ag(86)–ZSM-5	0.86		—	—	0.01	
Na–ZSM-5	—		0.0		1.0	
				0.09		0.25
Ce(9)–ZSM-5	—		0.03		0.75	
				0.12		0.02
Ce(21)–ZSM-5	—		0.07		0.73	
				0.21		0.11
Ce(42)–ZSM-5	—		0.14		0.62	
				0.12		0.08
Ce(54)–ZSM-5	—		0.18		0.54	

[a] All elements measured by ICP.
[b] Increment of silver ion-exchange level calculated from Column B.
[c] Increment of cerium ion-exchange level calculated from Column D.
[d] Decrease of residual sodium level calculated from Column F.

Ce^{3+} in various Ce–ZSM-5 and Ce–Cu–ZSM-5 materials prepared by the same ion exchange method and the same heat treatment as in this work. The Ce^{3+} luminescence intensity did not increase with Ce loading from Ce/Al = 0.035 to 0.2, implying that saturation of Ce^{3+} species was reached at relatively low exchange levels. In Table 4, the higher Ce exchange increments (column E) than the corresponding amount of Na^+ (column G) being exchanged out of the zeolite (except for the Ce(9)–ZSM-5 sample) indicates that cerium may exist in partially hydroxylated form, such as $[Ce(OH)_2]^+$ and $[Ce(OH)]^{2+}$. During the air-calcination step, oxidized cerium clusters can be formed on the zeolite surface. This is supported by surface Ce/Si ratios higher than the bulk in Fig. 10, as well as by the Ce clusters seen in the STEM/EDS mappings (Figs. 7b, 7d, and 9b) and in the HRTEM image (Fig. 8b) and the strong CeO_2 UV-VIS DR band at 294 nm (Fig. 12a). On the basis of HRTEM, the CeO_2 clusters are 1–3 nm in size. However, an amount of Ce^{3+} still remains, as verified by luminescence (29) and UV-VIS DRS (Fig. 12a). It is not clear how this Ce^{3+} is coordinated with oxygen in the zeolite structure.

Structure and Activity of Silver

The rate of NO reduction to N_2 over Ce–Ag–ZSM-5 increased linearly with the Ag ion exchange level up to Ag/Al ≈ 0.6 (Fig. 1a). Within this range, silver ions exchanged into the zeolite appear to be very effective for N_2 production, and the rate of the SCR reaction was higher than the rate of CH_4 oxidation by O_2 (Fig. 1a vs Fig. 4), resulting in high catalyst selectivity. At higher Ag loading, the rate of the SCR reaction leveled off (Fig. 1a), while the rate of the CH_4 combustion increased significantly (Figs. 1b and 4). As discussed above, Ag is well dispersed in the zeolite channels at low loadings, while at high Ag loadings, Ag particles (Figs. 7d and 8b) were found on the zeolite surface. Therefore, it can be concluded that dispersed Ag^+ ions and Ag particles have different catalytic properties for the SCR and CH_4 combustion reactions. The dispersed ionic state of silver is highly active and selective for the SCR reaction, while silver particles are nonselective and catalyze CH_4 combustion. Nanocrystalline (5–10 nm) silver particles on zirconia have been found to be very active for the complete oxidation of methane in recent work in our lab (43, 44). In a recent paper, Bethke and Kung (23) have similarly explained the low activity of a 6 wt% Ag/Al_2O_3 for the SCR reaction of NO with C_3H_6, i.e., metallic silver particles in this high Ag-content material catalyzed the combustion of propylene rather than the SCR reaction. The opposite was true for a low Ag-content sample, 2 wt% Ag/Al_2O_3, which contained silver in oxidized form.

The Role of Cerium

Ce–ZSM-5 as a catalyst for the SCR of NO by hydrocarbons has been studied extensively by Yokoyama and Misono (13, 25, 45) using propene as the reducing agent. The major function of Ce suggested in those studies was to initiate the SCR reaction by converting NO to NO_2. This function of cerium is also clearly manifested here in the Ce–Ag–ZSM-5 system for the SCR of NO with methane (Figs. 5 and 6). In Fig. 6, using NO_2 in the feed gas, at temperatures lower than 500°C where the gas-phase NO_2 concentration is sufficiently high, the activity of Ag–ZSM-5 was the same as that of Ce–Ag–ZSM-5. This indicates that once NO_2 is available, Ag–ZSM-5 is capable of converting NO_2 to N_2 at the same rate as the bi-metal Ce–Ag–ZSM-5 catalyst. In other words, the SCR of NO on Ag–ZSM-5 is limited by the availability of NO_2 and one function of Ce in Ce–Ag–ZSM-5 is to catalyze the NO oxidation to NO_2 (Fig. 5). The high-temperature deviation of the rate over Ag(77)–ZSM-5 from that over Ce(24)–Ag(78)–ZSM-5 (Fig. 6) may be explained by the decrease of gas-phase NO_2 concentration due to the equilibrium of $NO_2 \rightarrow NO$. But on Ce(24)–Ag(78)–ZSM-5, surface NO_2 species may be continuously formed on the Ce sites and continuously consumed on the Ag sites under steady-state conditions. The drop of the high-temperature catalyst activity when O_2 was removed from the feed gas stream (Fig. 6, dashed lines vs solid lines) further supports this explanation. We may also suggest that stable nitrite or nitrate species are formed on the cerium sites extending the SCR activity to higher temperatures similar to the findings by Sadykov *et al.* (46) on Ca–Fe–ZSM-5 and Sr–Cu–ZSM-5.

The dependence of SCR activity on the cerium exchange level shown in Fig. 2a can be explained in part by increased NO_2 supplied by cerium. The stronger dependence of the NO reduction rate on Ce/Al at higher temperatures (550 and 600°C) is probably due to the increasing importance of surface NO_2 species formed on the Ce sites. At these elevated temperatures, gas-phase NO_2 is less available as determined by thermodynamic equilibrium (Fig. 5), and surface NO_2 on the Ce sites may be the major source of this important reaction intermediate.

Characterization of Ce–ZSM-5 samples by UV-VIS DRS shows that both Ce^{3+} species and CeO_2 co-exist in the Ce–Ag–ZSM-5 catalysts. Oxidation of NO to NO_2 conducted over CeO_2 demonstrated that CeO_2 is an even better catalyst for oxidation of NO to NO_2 (18, 25). Therefore, we believe that CeO_2 formed on the catalyst surface may also contribute directly to the enhancement of the SCR reaction.

As discussed before, Ag^+ ions provide the main sites for the SCR reaction. In the presence of cerium, higher dispersion of silver was achieved as shown in Figs. 7d and 8b, especially at high Ag loadings. Migration of silver may, thus, be inhibited by cerium. Ag is stabilized by cerium and retained in dispersed oxidized state which favors the SCR reaction. All structural evidence from Ce–Ag–ZSM-5, namely, the lower extent of clustering shown in Figs. 7d and 8b, the lower surface Ag/Si ratio in Fig. 10, and the absence of the 420-nm metallic silver band in Fig. 12c, clearly shows cerium plays a major structural role in Ce–Ag–ZSM-5: it stabilizes silver in a highly dispersed and ionic state. A similar structural function of cerium has been reported in the Ce–Cu–ZSM-5 system for NO decomposition (16, 29).

Addition of cerium into Ag–ZSM-5 suppresses the activity of Ag–ZSM-5 for CH_4 combustion, as shown in Figs. 2b, 3, and 4. The rate of CH_4 oxidation over Ce-promoted Ag–ZSM-5 decreased also for the sample with Ag/Al = 0.22 (Table 3). In this material, silver initially existed in dispersed Ag^+ form even in the absence of cerium. At present, we do not have adequate data to explain the suppression of CH_4 combustion at low Ag/Al ratios. One possibility is that in the absence of cerium, the aggregation of silver may be fast at high temperature. As the Ag/Al ratio increased, i.e., when silver particles were formed, the rate of CH_4 combustion increased and approached that of the unpromoted Ag–ZSM-5 samples (Figs. 3 and 4). This is in line with the activity of metallic silver particles for hydrocarbon combustion, including methane (23, 33, 34, 43, 44).

CONCLUSION

Addition of a small amount of Ce in Ag–ZSM-5 promotes both the activity (rate of NO reduction to N_2) and the selectivity of the catalyst for the SCR of NO by CH_4 in the presence of excess oxygen. Different correlations between catalyst activity and Ce and Ag exchange levels were identified in this work for the CH_4–SCR reaction and CH_4 combustion. Increase of Ce loading to 1.5 wt% increases the rate of NO reduction to N_2, while it decreases the rate of methane combustion. Catalysts with high Ag ion exchange level (>50%) are more active for methane combustion, while those with low Ag loading are more effective for the SCR reaction.

The activity and selectivity of Ce–Ag–ZSM-5 for the SCR reaction are closely related to the dispersion and oxidation states of silver and cerium. Cerium is present in two oxidation states, 3+ and 4+, primarily in the form of CeO_2 clusters of 1–3 nm on the zeolite surface. Silver exists as isolated ions, clusters, and metallic particles of 8–12 nm on the zeolite surface. The dispersed silver state provides sites for the SCR reaction, i.e., the formation of N_2, while metallic Ag particles are active for CH_4 combustion.

The major functions of cerium in the Ce–Ag–ZSM-5 system have became clear in this work; namely cerium catalyzes the oxidation of NO to NO_2 and suppresses CH_4 combustion. Most importantly, the incorporation of cerium into Ag–ZSM-5 stabilizes silver ions and keeps them dispersed, thus suppressing the formation of silver particles, which are more active for the competing methane combustion reaction.

ACKNOWLEDGMENTS

We gratefully acknowledge the financial support of this work by the EPA under Contract G6J21469. We also thank Dr. Anthony Garratt-Reed, Mr. Michael Frongillo, and Ms. Elisabeth Shaw of the Center of Materials Science and Engineering at Massachusetts Institute of Technology for their assistance with the STEM/EDS, HRTEM/EDS, and XPS analyses.

REFERENCES

1. Iwamoto, M., "Proc. of Meeting of Catalytic Technology for Removal of Nitrogen Monoxide, Tokyo, 1990," pp. 17–22.
2. Held, W., Konig, A., Richter, T., and Puppe, L., SAE Paper 900496, 1990.
3. Lukyanov, D. B., Sill, G., d'Itri, J. L., and Hall, W. K., *J. Catal.* **153**, 265 (1995).
4. Witzel, F., Sill, G., and Hall, W. K., *J. Catal.* **149**, 229 (1994).
5. Li, Y., and Armor, J. N., U.S. Patent 5,149.512, Sept. 22, 1992.
6. Li, Y., and Armor, J. N., *Appl. Catal. B* **1**, L31 (1992).
7. Li, Y., and Armor, J. N., *J. Catal.* **145**, 1 (1994).
8. Kikuchi, E., Ogura, M., Aratani, N., Sugiura, Y., Hiromoto, S., and Yogo, K., *in* "Environmental Catalysis" (G. Centi, *et al.*, Eds.), p. 29. SCI Publ., Rome, Italy, 1995.
9. Yogo, K., and Kikuchi, E., *Stud. Surf. Sci. Catal.* **84**, 1547 (1994).
10. Descorme, C., Gelin, P., Lecuyer, C., and Primet, M., *Appl. Catal. B* **13**, 185 (1997).
11. Pereira, C. J., and Amiridis, M. D., *in* "ACS Symposium Series 587" (U. Ozkan, S. Agrawal, and G. Marcelin, Eds.), p. 1. American Chem. Soc., Washington, DC, 1994.
12. Teraoka, Y., Ogawa, H., Furukawa, H., and Kagawa, S., *Catal. Lett.* **12**, 361 (1992).
13. Yokoyama, C., and Misono, M., *Bull. Chem. Soc. Jpn.* **67**, 557 (1994).
14. Torre-Abreu, C., Riberio, M. F., Henriques, C., and Ribeiro, F. R., *Catal. Lett.* **43**, 25 (1997).
15. Zhang, Y., Sun, T., and Flytzani-Stephanopoulos, M., *in* "ACS Symposium Series 587" (U. Ozkan, S. Agrawal, and G. Marcelin, Eds.), p. 133. American Chem. Soc., Washington, DC, 1994.
16. Zhang, Y., Sc.D thesis, MIT, Cambridge, MA, 1995.
17. Parvulescu, V. I., Oelker, P., Grange, P., and Delmon, B., *Appl. Catal. B* **16**, 1 (1998).
18. Li, Z., Ph.D. thesis, Tufts University, 1998.
19. Li, Z., and Flytzani-Stephanopoulos, M., *Appl. Catal. A* **165**, 15 (1997).
20. Han, S., Martenak, D. J., Palermo, R. E., Pearson, J. A., and Walsh, D. E., *J. Catal.* **148**, 134 (1994).
21. Li, Y., and Armor, J., *Appl. Catal. B* **3**, 275 (1994).
22. Miyadera, T., and Yoshida, K., *Chem. Lett.*, 1483 (1993); *Appl. Catal. B* **2**, 199 (1993).
23. Bethke, K. A., and Kung, H. H., *J. Catal.* **172**, 93 (1997).
24. Masuda, K., Tsujimura, K., Shinoda, K., and Kato, T., *Appl. Catal. B* **8**, 33 (1996).
25. Yokoyama, C., and Misono, M., *Catal. Lett.* **29**, 1 (1994).
26. Hamada, H., Kintach, Y., Sasaki, M., Ito, T., and Tabata, M., *Appl. Catal.* **70**, L15 (1991).
27. Li, Y., Salager, T. L., and Armor, J. N., *J. Catal.* **150**, 338 (1994).
28. Haneda, M., Kintaichi, Y., Inaba, M., and Hamada, H., *Bull. Chem. Soc. Jpn.* **70**, 499 (1997).
29. Zhang, Y., and Flytzani-Stephanopoulos, M., *J. Catal.* **164**, 131 (1996).
30. Texter, J., Hastrelter, J. J., and Hall, J. L., *J. Phys. Chem.* **87**, 4690 (1983).
31. Brown, D. R., and Keven, L., *J. Phys. Chem.* **90**, 1129 (1986).
32. Matsuoka, M., Matsuda, E., Tsuji, K., Yamashita, H., and Anpo, M., *Chem. Lett.*, 375 (1995).
33. Pestryakov, A. N., Davydov, A. A., and Kurina, L. N., *Russian J. Phys. Chem.* **60**, 1251 (1986).
34. Bogdanchikova, N. E., Dulin, M. N., Toktarev, A. V., Shevnina, G. B., Kolomiichuk, V. N., Zaikovskii, V. I., and Petranovskii, V. P., *Stud. Surf. Sci. Catal.* **84**, 1067 (1994).
35. Ershov, B. G., Janata, E., and Henglein, A., *J. Phys. Chem.* **97**, 339 (1993).
36. Pestryakov, A. N., and Davydov, A. A., *Appl. Catal. A* **120**, 7 (1994).
37. Beyer, H., Jacobs, P. A., and Uytterhoven, J. B., *J. Chem. Soc. Faraday Trans. I* **72**, 674 (1976).
38. Viana, B., Aka, G., Vivien, D., Lejus, A. M., Thery, J., Derory, A., Bernier, J. C., Garapon, C., and Boulon, G., *J. Appl. Phys.* **64**, 1398 (1988).
39. Bensalem, A., Muller, J. C., and Bozon-Verduraz, F., *J. Chem. Soc. Faraday Trans.* **88**, 153 (1992).
40. Bensalem, A., Bozon-Verduraz, F., Delamar, M., and Bugli, G., *Appl. Catal. A* **121**, 81 (1995).
41. Ali, A., Alvarez, W., Loughran, C. J., and Resasco, D. E., *Appl. Catal. B* **14**, 13 (1998).
42. Nishizaka, Y., and Misono, M., *Chem. Lett.*, 2237 (1994).
43. Kundakovic, L., and Flytzani-Stephanopoulos, M., *J. Catal.* **179**, 203 (1998).
44. Kundakovic, L., Ph.D. thesis, Tufts University, 1998.
45. Yokoyama, C., and Misono, M., *J. Catal.* **160**, 95 (1996).
46. Sadykov, V. A., Baron, S. L., Matyshak, V. A., Alikina, G. M., Bunina, R. V., Rozovskii, A. Ya., Lunin, L. L., Lunina, E. V., Kharlanov, A. N., Ivanova, A. S., and Veniaminov, S. A., *Catal. Lett.* **37**, 157 (1996).